Research on the Inversion Method of Geostress Field in a Certain Block of Daqing

Geng Liu
School of Mechanical Science and Engineering, Northeast Petroleum University, Daqing, China

Abstract: The geostress field is crucial for oil and gas resource evaluation, oil and gas reservoir exploitation, drilling and completion engineering, etc. It is crucial to clarify the distribution of geostress and grasp the magnitude and direction of geostress. This study focuses on a certain block in Daqing Oilfield and uses seismic, logging, and geological data to establish a three-dimensional geological structure, fault, natural fracture, and attribute model on the Petrel platform. The stress field is simulated using finite element theory. Research has found that faults and cracks significantly affect the stress field, leading to changes in size and direction. The distribution range of principal stress is 40-55MPa and 40-58MPa, with vertical stress ranging from 40-70MPa. The simulation results verify reliability and provide a foundation for future fracturing construction. These findings will help to better evaluate underground conditions and guide the development of oil and gas resources.

Keywords: Geostress Field; Petrel; Numerical Simulation; Shale; Fault

1. Introduction

The geostress field serves as a primary basis for assessing formation fracture pressure, collapse pressure, wellbore trajectory design, and hydraulic fracturing design. It predominantly encompasses the effects on fracture initiation pressure and fracture strike, directly influencing the enhancement of hydraulic fracturing production, impacting wellbore stability, casing integrity, and the layout of injection-production well networks.

Numerous scholars have attempted to model the geostress field in different blocks using various methods and technologies. In 2005, Chen et al. [1] estimated geostress values using logging data as a substitute for measured geostress values to calculate stresses in the Pubei reservoir of Daqing. This approach relies on the quantity and quality of the measurement data; inadequate or poor-quality data can severely impact the results of the stress field simulation. In 2011, Zhang et al. [2] conducted numerical simulations of complex block geostress fields using Abaqus and Petrel software. In 2021, Zhang et al. [3] modeled the geostress field of the 403x1 block in the Nanpu Oilfield using Petrel and ANSYS software. However, the numerical simulation method faces challenges such as model exporting and importing issues, involving intricate procedures and vast amounts of data processing. In 2021, Zhao et al. [4] utilized a shear wave travel time prediction model and the kriging interpolation method to model the geostress field in a work area, although this method did not address the issue of geostress field orientation. In 2021, Wang et al. [5] used logging interpretation and three-dimensional numerical simulation to identify the spatial distribution characteristics of the current stress field in the Qingshankou Formation of the Gulong Shale in the Songliao Basin. The method showed significant differences in the direction of the maximum horizontal principal stress near the wellbore. In 2021, Liang et al. [6] referenced hydraulic fracturing renovation data and logging data to construct a 3D spatial numerical model using seismic constraints and performed inversion of the 3D geostress field in the work area based on single-well geostress. However, there were certain errors in determining the orientation of the maximum horizontal principal stress at different well locations. In 2022, Chen et al. [7] established a three-dimensional detailed geostress field in a specific block in the Shunbei Oilfield using a method that involved comparing and analyzing 3D geological models with single-well geostress. Nonetheless, this method exhibited a high dependency on logging data.

In response to the aforementioned challenges, this study utilizes seismic data, logging data,

Copyright @ STEMM Institute Press

and geological information to establish a three-dimensional geological structure model, attribute model, and finite element geomechanical grid using the Petrel software. By defining simulation block pressures, temperatures, saturations, and stress boundary conditions, the geostress field simulation in the study area is conducted to provide a foundation for hydraulic fracturing operations.

2. Analysis of Target Blocks

The Songliao Basin, located in the northeastern region of China with an area of approximately 260,000 square kilometers, is one of the most abundant onshore oil and gas basins in China. The basin features a typical continental fault depression with subsequent sag; the central sag comprises secondary structural units such as Qijia-Gulong, Daqing Changyuan, and Sanzhao, making it a prime exploration and development target area. The study block is situated within the Gulong syncline zone, a secondary structural belt within the Qijia-Gulong sag in the northern part of the central basin. The region includes three major fault systems: the northern, western, and eastern faults, with a dense network of natural fractures. The shale oil in the study block is primarily developed in the Qingshankou Formation Qing 1 section and Qing 2 section, comprising nine oil layers labeled Q1 to Q9 from bottom to top. These layers represent mid to high maturity shale oil and serve as the main target reservoirs for current exploration and development efforts.

3. One-dimensional Geostress Analysis

3.1 Vertical Geostress Analysis

Vertical geostress refers to the stress caused by the weight of overlying rocks, expressed by the following equation:

$$\sigma_v = \int \rho g dh \quad (1)$$

Where,

ρ = the density value from logging in kg/m³;

g= the acceleration due to gravity in m/s²;

h= the thickness of the strata in meters.

The calculation results indicate that the distribution of vertical stress ranges from 40 to 70 MPa, with an average value of 58 MPa.

3.2 Horizontal Geostress

Hydraulic fracturing presently stands as the conventional method for measuring geostress [8], involving calculations of geostress based on the stress state of the wellbore and the fracturing mechanism. According to rock mechanics theory, when the fluid density within the wellbore exceeds a certain threshold, causing the stress imposed on the rock to precisely exceed its tensile strength, the formation fractures. At this juncture, the fracturing pressure can be determined:

$$P_f = 3\sigma_h - \sigma_H - \alpha P_p + S_t \quad (2)$$

During the fracturing process, the closure pressure reflects the magnitude of the minimum horizontal principal stress. By reading the closure pressure and fracturing pressure from the fracturing construction curve, the maximum horizontal principal stress can be calculated according to equation (2). The rock tensile strength, Biot coefficient, and formation pore pressure in equation (2) are all derived from experimental test results. In equation (2), σ_H represents the maximum horizontal principal stress in MPa; σ_h denotes the minimum horizontal principal stress in MPa; P_f is the fracturing pressure in MPa; α is the Biot coefficient; P_p is the formation pore pressure in MPa; and S_t stands for the rock tensile strength in MPa. Through analyzing fracturing data in the research area, one can obtain the fracturing pressure and closure pressure at fracturing depths, thereby calculating the corresponding maximum and minimum horizontal principal stresses. The computed outcomes reveal that the minimum horizontal principal stress ranges from 40 to 55 MPa, with an average of 50 MPa; while the maximum horizontal principal stress ranges from 40 to 58 MPa, averaging at 51 MPa.

3.3 Direction of Geostress

The direction of geostress is typically determined through Formation Micro-Imager (FMI) logging combined with borehole image and six-arm caliper logging. Throughout the drilling process, as the wellbore rock cores are extracted, stress concentration occurs on the wellbore wall, inducing fractures. If this stress concentration exceeds the rock's surrounding fracture strength, wall collapse may ensue [9]. This method reveals the strike of induced fractures, which corresponds to the direction of maximum horizontal principal stress (see Figure 1), with the long axis of the collapse ellipse aligning parallel to the direction of the

 Copyright @ STEMM Institute Press

minimum horizontal principal stress. In the evaluated block, the strike of induced fractures in the interval from 2,443 to 2,446 meters is 90°, leading to the determination that the maximum horizontal principal stress direction in this well is 90°.

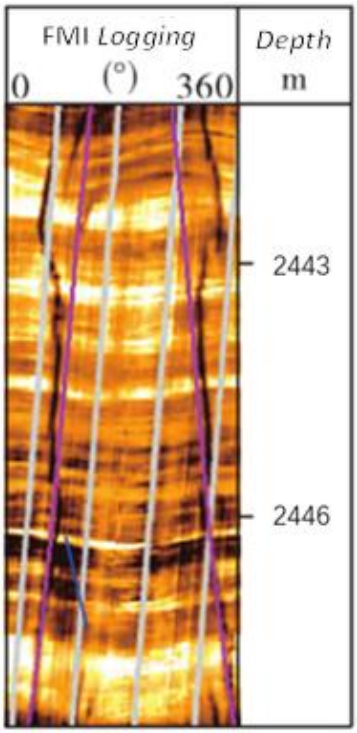

Figure 1. Direction of Geostress

4. Modeling of the Study Block Structure

4.1 Structural Modeling of the Study Block

The study block consists of shale reservoirs, characterized by intricate geological structures and encompasses 16 fault lines with a dense network of natural fractures. The presence of these faults and natural fractures results in a complex distribution of geostress in the study block, making precise predictions challenging. Leveraging seismic data, logging information, and geological data, this study utilizes the Petrel platform to accomplish three-dimensional geological structural modeling, fault modeling, and natural fracture modeling of the study block. The study area extends 4,400 meters in the I direction, 6,900 meters in the J direction, and has a height of 140 meters in the K direction, encompassing a total of 9 major layers from Q9 to Q1. The model is established using the corner-point grid method [10], comprising a total of 2,101,200 grids and 2,473,570 nodes as illustrated in Figure 2.

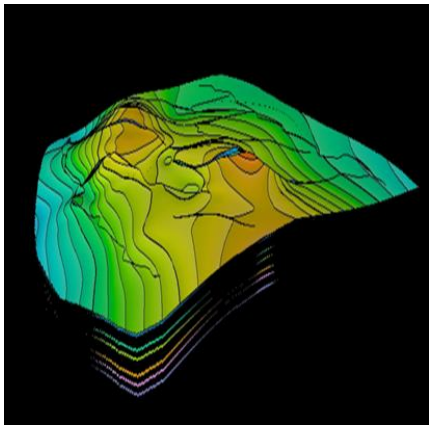

Figure 2. 3D Geological Model

4.2 Processing of Logging Data and Establishment of Attribute Models

Geological parameters form the foundational elements for studying the geostress field, encompassing critical factors like Young's modulus, Poisson's ratio, density, compressive strength, tensile strength, internal friction angle, porosity, and permeability. In this research endeavor, the curation of logging curves commences with the meticulous removal of outliers, both maximum and minimum values, followed by data refinement based on empirical equations and computational principles drawn from referenced literature [11]. Subsequently, the refined data undergoes a systematic sequential Gaussian simulation [12] method, culminating in the development of the attribute volumetric model for the study block, as illustrated in Figure 3 and 4. This model assessment reveals a nuanced landscape of heterogeneity; where Young's modulus gracefully fluctuates between 20 and 30 GPa, Poisson's ratio delicately oscillates within the range of 0.23 to 0.31, and the density profile exhibits a notably uniform distribution, close to 2.6g/cm^3.

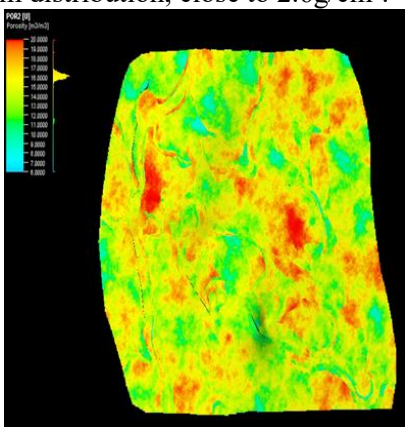

Figure 3. Permeability Model

Copyright @ STEMM Institute Press

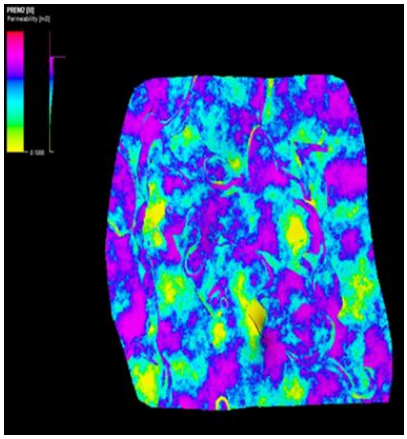

Figure 4. Porosity Model

4.3 Three-dimensional Modeling of the Geostress Field

Utilizing the finite element method [13] for numerical simulation of the geostress field entails discretizing the entire geological volume into a finite number of interconnected nodes forming continuous elements. Each element is assigned corresponding geological parameters, thereby transitioning from the solution of a continuous field function within the study block to the solution of a discrete set of field points. The establishment of a three-dimensional structural model and attribute model lays the groundwork for geostress field modeling. To avoid stress concentration during modeling, it is essential to include overlying strata, underlying strata, surrounding rock layers, and so forth within the study area. These additional areas are endowed with pertinent rock mechanics parameters to closely resemble real geological formations. Subsequently, pressure, temperature, boundary conditions, and other simulation parameters are defined to simulate operational scenarios. The specific procedures are delineated in Figure 5

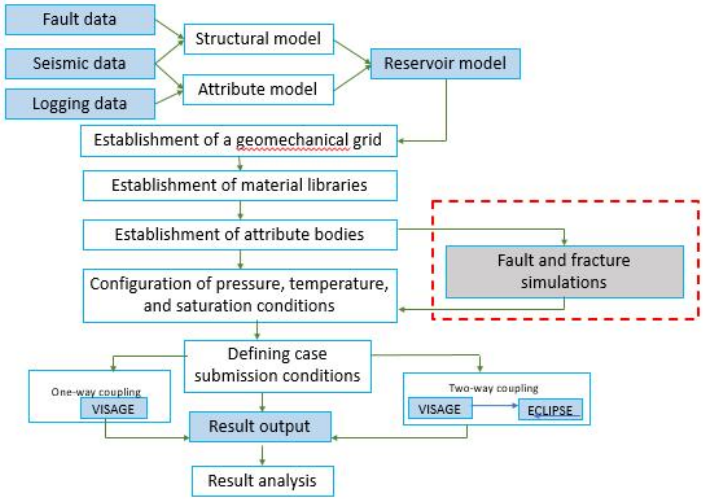

Figure 5. Modeling Process

4.3.1 Establishment of the geomechanical grid

Having already constructed the three-dimensional geological model, the subsequent step involves building the overlying strata, underlying strata, surrounding rock layers, and rigid elements to prevent stress concentration and ensure uniform boundary load distribution. The geomechanical grid extends outward using a proportional scaling approach, with the overall model width-to-depth ratio not exceeding 3:1, as illustrated in Figure 6. The geomechanical grid extends outward using a proportional scaling approach, with the overall model width-to-depth ratio not exceeding 3:1, as illustrated in Fig. 6. Upon completion of the geomechanical grid establishment, a total of 830,820 grid cells and 892,100 nodes have been generated. Taking into account engineering scale considerations and computational capabilities, the grid is coarsened without compromising computational precision.

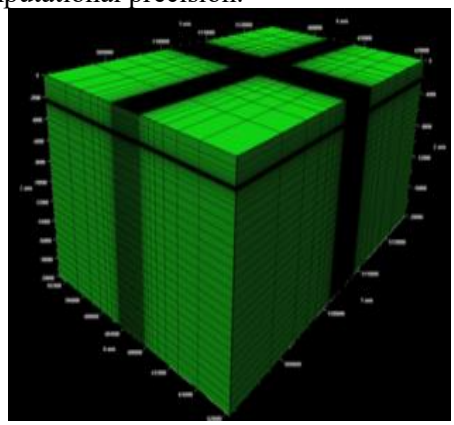

Figure 6. Geomechanical Grid

 Copyright @ STEMM Institute Press

4.3.2 Establishment of material library and attribute models

The material library encompasses a comprehensive set of named parameters and values, defining rock types (such as sandstone, shale, etc.) and specifying corresponding rock mechanics parameters (Young's modulus, Poisson's ratio, rock density, compressive strength, etc.), along with elastic models and yield criteria. This model comprises two main categories of materials: intact rock masses (defining elastic models and yield criteria) and discontinuous bodies (including faults, fractures, specifying stiffness, strength, and spacing). During the segmentation of the geomechanical grid, five sections were delineated: overlying strata, underlying strata, surrounding rock layers, study blocks, and rigid elements, all of which pertain to intact rock masses. Faults and natural fractures constitute discontinuous bodies, with corresponding parameter settings detailed in Tables 1 and 2. For the established material library, it is imperative to assign property values to the respective regions. While the study block is overlaid with various attribute bodies established earlier, other sections are covered using the values outlined in the tables below.

Table 1. Complete Rock Mechanics Parameters of Rock Mass

	Young's modulus /Gpa	Poisson's ratio	Density/g*cm-3
Overlying strata	10	0.28	2.3
Underlying strata	10	0.23	2.32
Study blocks	20～30	0.23～0.31	2.0~2.72
Surrounding rock layers	25	0.25	2.3
Rigid elements	50	0.23	2.3

Table 2. Mechanical Parameters of Discontinuous Rock

	Normal stiffness /Gpa	Shear stiffness /Gpa	Frictional angle/°
Faults	0.4	0.15	20
Natural fractures	8	4	20

4.3.3 Configuration of pressure, temperature, and boundary conditions

The term "pressure" in this context refers to reservoir pore pressure [14]. In this study, the Petrel platform's Intersect plugin is utilized for reservoir simulation within the study blocks, enabling the derivation of pore pressure attribute bodies. The temperature is set at 100°C. Through methods such as wellbore collapse and induced fracturing during drilling, the maximum horizontal principal stress direction in the study area is determined to be near the east direction. Consequently, for numerical simulation, the maximum horizontal principal stress direction is set at NE90° and it is assumed that the principal stress direction remains constant with depth. Based on differential strain experiments, the maximum horizontal principal stress gradient in the study block is determined to be 0.02 MPa/m, while the minimum horizontal principal stress gradient is 0.018 MPa/m. Vertical geostress is automatically applied by the software, aligning closely with the actual stress conditions experienced by the study block within the crust.

4.3.4 Defining case submission scenarios

By importing geological parameters, pore pressure, boundary conditions, and other data into the VISAGE simulator, this study adopts a unidirectional coupling mode. It aims to compute the alterations in stress fields, deformation, and displacements resulting from faults and natural fractures, thereby capturing the intricate geomechanical responses within the system.

4.3.5 Simulation result analysis

Through finite element numerical simulations, the geostress field distribution within the study block is obtained, encompassing the tridirectional principal stresses: the maximum horizontal principal stress (σ_H), the minimum horizontal principal stress (σ_h), and the vertical principal stress (σ_V) in terms of their orientations and magnitudes (refer to Figure 7). It is discerned from the graphical representations that the three-dimensional stress field undergoes deviations in direction and alterations in magnitude due to the influences of faults and natural fractures. The simulation reveals the following distributions: the minimum horizontal principal stress ranges from 46 to 55 MPa, bearing proximity to the south direction; the maximum horizontal

Copyright @ STEMM Institute Press

principal stress ranges from 48 to 59 MPa, aligned with the east direction; and the vertical stress spans from 40 to 70 MPa. Upon comparison with field measurements, the simulation results exhibit minimal discrepancies (refer to Figure 8), particularly in the orientation of the maximum horizontal principal stress, with stress field numerical simulation errors (refer to Table 3) remaining within 15%.

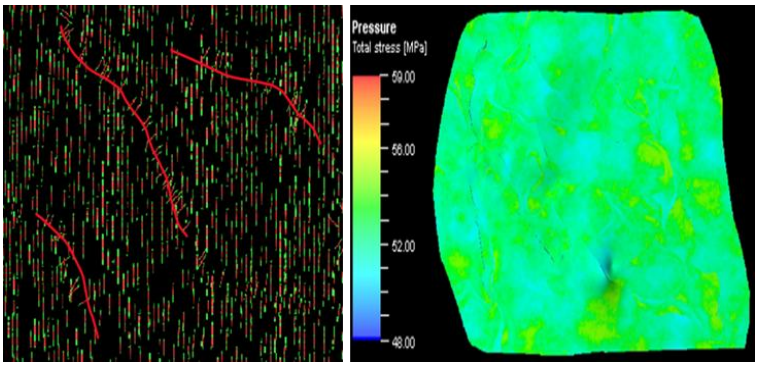

a. Maximum horizontal principal stress distribution

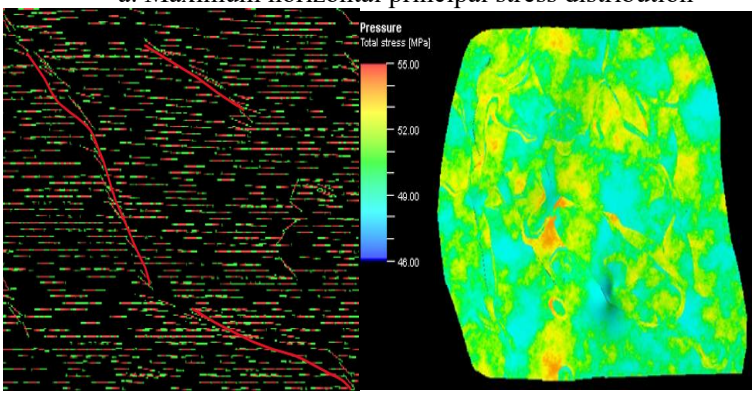

b. Minimum horizontal principal stress distribution

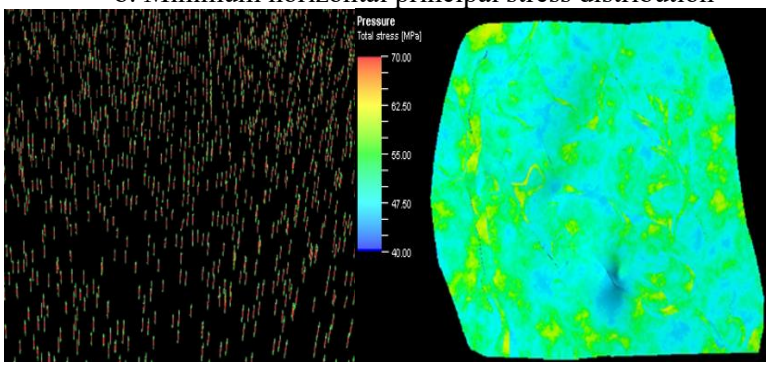

c. Vertical stress distribution

Figure 7. Direction and Magnitude of Three-dimensional Stress

Table 3. Comparison between Three-dimensional Stress and Single Well Values

Depth/m	σ_H/Mpa		σ_h/Mpa		σ_v/Mpa		Error/%		
	Simulation	Single well	Simulation	Single well	Simulation	Single well	σ_H	σ_h	σ_v
3000	46.25	51.01	48.17	54.65	57.87	58.97	-9.33	-11.86	-1.87
4000	47.09	54.84	50.43	56.84	60.75	59.09	-14.2	-11.28	2.81
5000	48.64	52.23	49.56	55.79	59.88	58.25	-6.87	-11.17	2.80

Guided by the geostress field characteristics of the study block, the hydraulic fracturing design within this area involves drilling horizontal wells along the direction of the minimum principal stress and orienting perforations along the direction of the maximum principal stress. Utilizing the K-Netix module in Petrel software, numerical simulations are conducted for a specific well within the operational zone. Section 1 exhibits a fracture length of 256 meters, a fracture height of 12 meters, and a fracture width of 2.3 millimeters (see Figure 8), in conjunction with microseismic monitoring [15] results (refer to

 Copyright @ STEMM Institute Press

Fig.ure 9). Comparing the data from this well with early hydraulic fracturing data within the study block, significant improvements are observed in terms of fracture length and height.

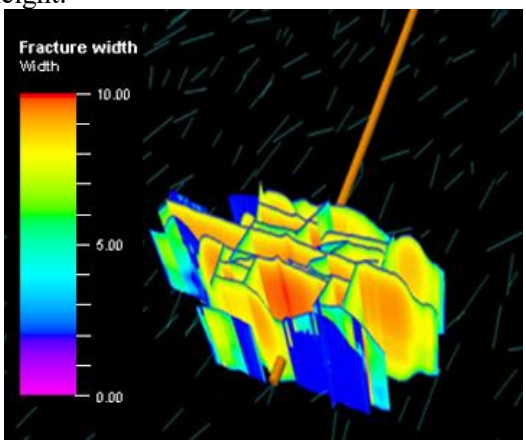

Figure 8. Numerical Simulation of Fracturing in Section 1

4.3.6 Application of geostress field simulation

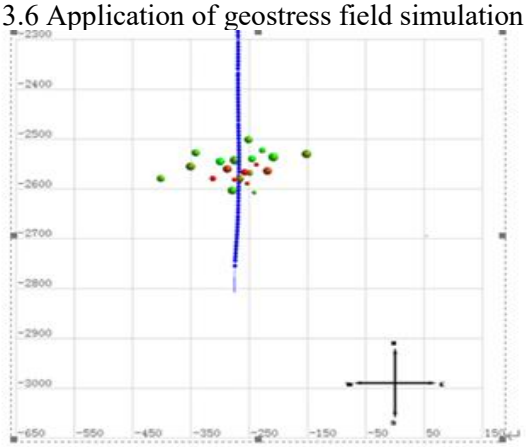

Figure 9. Microseismic Monitoring Results

5 Conclusion

By establishing a three-dimensional geological model of the study block using the Petrel platform and taking into account factors such as faults and natural fractures, a comprehensive simulation of the geostress field within the study area was conducted. A comparison between field measurements and simulation results revealed that while the directional errors in the geostress field of the study block are minimal, numerical errors remain within an acceptable range of 15% in engineering applications.

(1) The distribution of the minimum horizontal principal stress ranges from 46 to 55 MPa, in the vicinity of the south direction; the distribution of the maximum horizontal principal stress ranges from 48 to 59 MPa, close to the east direction; and the vertical stress distribution spans from 40 to 70 MPa.

(2) Faults and natural fractures have an impact on the stress field in their vicinity, leading to significant alterations in stress magnitude and deviations in direction.

(3) This study has addressed the complexities associated with constructing models for simulating the geostress field, as well as the laborious tasks of data organization, export, and import, streamlining these processes for greater efficiency.

References

[1] Chen Zhaowei, Cai Yong'en, Yin Youquan, et al. Stress Field Inversion Analysis of Pubei Reservoir in Daqing// Chinese Society of Mechanics, Beijing University of Technology. Academic Conference of Chinese Society of Mechanics, 2005:672.

[2] Zhang Guangming, Xiong Chunming, Liu He, et al. Numerical simulation method for in-situ stress field in complex fault block. Fault-Block Oil and Gas Field, 2011, 18(06):710-713.

[3] Zhang Yang, Wu Haitao, Duan Bin, et al. Modeling and Application of Heterogeneous Stress Field in Fault-Block Type Low-Permeability Reservoirs: A Case Study of Block 403X1 in Nanpu Oilfield. Journal of Shandong Institute of Petroleum and Chemical Technology, 2021, 35(04):13-19.

[4] Zhao Xuyang, Guo Haimin, Li Zixuan, et al. Modeling of in-situ stress field and rock mechanics parameters based on logging shear wave prediction. Fault-Block Oil and Gas Field, 2021, 28(02):235-240.

[5] Wang Yongzhuo, Wang Rui, Dai Xu, et al. Design method for development of horizontal well casing for Gulong shale oil in the Songliao Basin. Daqing Petroleum Geology and Development, 2021,40 (05): 157-169

[6] Liang Lixi, Gao Yang, Liu Xiangjun, et al. Research on In-situ 3D Stress Field in Glutenite Formation. Science Technology and Engineering, 2021, 21(06):2194-2201.

[7] Chen Xiuping, Shen Xinpu, Liu Jingtao, et al. Refined finite element modeling and analysis of 3 D geostress field for a certain block in Shunbei oil field. Journal of Shenyang University of Technology, 2022, 44(05):595-600.

Copyright @ STEMM Institute Press

[8] Chen Wenting, Zheng Zhibin, Peng Yanyan. Application of Hydraulic Fracturing Method in In-situ Stress Measurement. Coal Technology, 2020, 39(02):66-68. DOI:10.13301/j.cnki.ct.2020.02.021

[9] Xia Wenhe, Zhu Zhehao, Han Yujiao, et al. Intelligent identification and segmentation method of wellbore fractures in resistivity logging imaging map. Oil Geophysical Prospecting, 2023, 58(05):1042-1052. DOI:10.13810/j.cnki.issn.1000-7210.2023.05.002

[10] Liu Yuyang, Liu Shiqi, Pan Mao, et al. Research of Crustal Stress Simulation Using Finite Element Analysis Based on Corner Point Grid. Acta Scientiarum Naturalium Universitatis Pekinensis, 2019, 55(04):643-653. DOI:10.13209/j.0479-8023.2019.020

[11] Zoback M D. Reservoir geomechanics. Cambridge: Cambridge University Press, 2007.

[12] Xiao Xiaonan. Multi-information Stochastic Dynamic Synthetical Optimization Simulation in Reservoir Description and Application Analysis of Intelligent Modeling. Journal of Xi'an Shiyou University (Natural Science Edition), 2021, 36(02):38-43.

[13] Tian Yiping, Liu Xiong, Li Xing, et al. Finite Element Method of 3-D Numerical Simulation on Tectonic Stress Field. Earth Science (Journal of China University of Geosciences), 2011, 36(02):375-380.

[14] Wu Furong, Zhou Shiyu, Deng Xiaojiang, et al. An improved seismic-constrained multi-factor pore pressure prediction method for shale gas reservoirs. Natural Gas Industry, 2021, 41(01):198-204.

[15] Liao Wei, Wei Lulu, Luo Haitao, et al. Application of microseismic monitoring in evaluation of geological body integrity for UGS in oil-gas fields. Oil Geophysical Prospecting, 2023, 58(04):913-921. DOI:10.13810/j.cnki.issn.1000-7210.2023.04.016.

 Copyright @ STEMM Institute Press